tion in the dye; nuclear/bath fluorescence = 0.35 ± 0.09, n = 5). The addition of $InsP_3$ to extruded nucleoplasm did not change the calcium green fluorescence (n = 3), indicating that the lack of fluorescence from the nucleus after $InsP_3$ application was not caused by a direct interaction between components of the nucleoplasm and $InsP_3$. These results eliminate the possibility that the nuclear matrix was necessary for dye exclusion and suggest that the envelope itself regulates transit of intermediate-sized (10 kD) molecules.

Although intermediate-sized molecules of ~10 kD were excluded by the nuclear envelope when the nuclear cisterna Ca^{2+} store was emptied, smaller molecules were not. Intact nuclei were Ca^{2+}-depleted by incubation in 10 nM Ca^{2+} solution with 1 μM $InsP_3$ for 3 min. Nuclei were exposed to a low molecular weight form of Lucifer yellow (500 daltons). Within 2 min after the addition of Lucifer yellow, nuclei had roughly the same fluorescence intensity as the bath (nuclear/bath = 0.84 ± 0.04, n = 8). To determine whether ions were excluded from nuclei, we loaded intact nuclei with the salt form of indo-1 and the nuclear Ca^{2+} store depleted with $InsP_3$. After depletion of stores, 100 μM Mn^{2+} was added to the bath and the fluorescence within the nucleoplasm was monitored. All fluorescence in the nucleoplasm was quenched with the addition of Mn^{2+}, without regard to the amount of Ca^{2+} within the store. In fact, the rate of quench and final fluorescence values were not statistically different in conditions of Ca^{2+}-filled (Fig. 1C) or Ca^{2+}-depleted nuclear stores (n = 8) (Fig. 4C). Lower [Mn^{2+}] (<1 μM) had similar effects (n = 4). Taken together, the results suggest that the nuclear Ca^{2+} store regulates the movement of molecules of ~10 kD, but not smaller molecules or ions.

Our results demonstrate that the nuclear Ca^{2+} store regulates size-specific entry of molecules into the *Xenopus* oocyte nucleus, including intermediate-sized molecules (10 kD) lacking an NLS that were previously thought to pass freely through the nuclear pore complex. We demonstrated that (i) movement of 10-kD molecules across the nuclear envelope depended on Ca^{2+} within the nuclear cisterna; (ii) depletion of this store was sufficient to halt diffusion across the envelope and did not require the nuclear matrix; and (iii) molecules and ions <500 daltons crossed the nuclear envelope regardless of the state of the nuclear Ca^{2+} store. The mechanism by which store depletion is sensed by the nuclear pore is unknown, but the nuclear pore protein, gp210, contains multiple Ca^{2+}-binding domains predicted to reside within the nuclear cisternae (*11*). Such a molecule might sense depletion of the nuclear cisternal [Ca^{2+}] and initiate conformational changes that block intermediate-sized molecule diffusion into the nucleus.

REFERENCES AND NOTES

1. C. Dingwall and R. Laskey, *Science* **258**, 942 (1992); C. Dingwall, *BioEssays* **13**, 213 (1991).
2. L. Davis, *Curr. Opin. Cell Biol.* **4**, 424 (1992).
3. C. W. Akey, *J. Cell Biol.* **109**, 955 (1989).
4. E. C. Hurt, *FEBS Lett.* **325**, 76 (1993).
5. M. S. Moore and G. Blobel, *Cell* **69**, 939 (1992); M. Stewart, *Cell Biol.* **3**, 267 (1992); M. A. Powers and D. J. Forbes, *Cell* **79**, 931 (1994).
6. I. Lang, M. Scholz, R. Peters, *J. Cell Biol.* **102**, 1183 (1986); L. Gerace and B. Burke, *Annu. Rev. Cell Biol.* **4**, 335 (1988); P. A. Silver, *Cell* **64**, 489 (1991).
7. L. Stehno-Bittel, A. Luckhoff, D. E. Clapham, *Neuron* **14**, 163 (1995).
8. D. O. Mak and J. K. Foskett, *J. Biol. Chem.* **269**, 29375 (1994).
9. P. Nicotera, S. Orrenius, T. Nilsson, P. O. Berggren, *Proc. Natl. Acad. Sci. U.S.A.* **87**, 6868 (1990); A. N. Malviya , P. Rogue, G. Vincendon, *ibid.*, p. 9270.
10. G. Grynkiewicz, M. Poenie, R. Y. Tsien, *J. Biol. Chem.* **260**, 3440 (1985); T. J. Hallam and T. J. Rink, *FEBS Lett.* **186**, 175 (1985); C. Lin, G. Hajnoczky, A. P. Thomas, *Cell Calcium* **16**, 247 (1994).
11. U. F. Greber and L. Gerace, *J. Cell Biol.* **128**, 5 (1995).
12. O. Bachs and N. C. E. Agell, *Biochim. Biophys. Acta* **1113**, 259 (1992).
13. *Xenopus laevis* oocytes were removed from toads as described [J. D. Lechleiter and D. E. Clapham, *Cell* **69**, 283 (1992)]. The salt form of fluorescent dyes was injected (50 nl of 1.0 mM dye/oocyte) into oocytes. After 30 min, defolliculated oocytes were enucleated manually by bisecting the oocyte along its equator. Nuclei were removed and washed of cytoplasm in mock intracellular solution containing 140 mM KCl, 10 mM Hepes, 3 mM $MgCl_2$ (pH 7.2). Loading of the nuclear cisterna with membrane-permeant fluorescent dyes was accomplished by incubating the isolated nucleus in mock intracellular solution containing the 100 μM AM form of dye for 15 to 30 min. All fluorescent molecules were purchased from Molecular Probes (Eugene, OR). Nuclei were imaged on a Bio-Rad confocal microscope as described (*8*) or on a Zeiss LSM-410 Laser Scanning confocal microscope. The light source was an argon/krypton laser tuned to either 360 or 488 nm. Two-dimensional confocal images were acquired by scanning 256 by 256 pixels per image. The effective thickness of the confocal optical section was controlled by varying the opening of a pinhole aperture in the detection path. Images were taken every 2 to 5 s, depending on the protocol, with a gray scale value for fluorescence intensity from 1 to 255. Images were processed on a Silicon Graphics Iris computer with ANALYZE software (Mayo Foundation). Background fluorescence values were subtracted in pseudocolor images (Figs. 1 and 3); black represents 0 and blue represents ~1 to 35 arbitrary pixel intensity units. Pixel values were averaged from within the nucleus and divided by the average pixel value of the bath. A ratio value of 1 indicated that fluorescence was equivalent in the nucleus and the bath. Results were expressed as means ± SEM. All experiments were done at room temperature (22° ± 2°C).
14. Nuclear ghosts were formed most commonly by positioning a small air bubble at the end of a micropipette and placing it in contact with the surface of isolated nuclei. Other methods included manually removing the nucleoplasm with a glass micropipette used for microinjection of mammalian cells. Typically, the nucleoplasm required 10 to 15 min to completely exit the nuclear envelope.
15. G. Schlenstedt, E. Hurt, V. Doye, P. A. Silver, *J. Cell Biol.* **123**, 785 (1993).
16. P. L. Paine, M. E. Johnson, Y. T. Lau, L. J. M. Tluczek, D. S. Miller, *BioTechniques* **13**, 238 (1992).
17. M. S. Schmidt-Zachmann, C. Dargemont, L. C. Kuhn, E. A. Nigg, *Cell* **74**, 493 (1993).

18. Supported by NIH grant 41303 to D.E.C.

10 July 1995; accepted 18 October 1995

A Nucleic Acid Triple Helix Formed by a Peptide Nucleic Acid–DNA Complex

Laurie Betts, John A. Josey,* James M. Veal, Steven R. Jordan

The crystal structure of a nucleic acid triplex reveals a helix, designated P-form, that differs from previously reported nucleic acid structures. The triplex consists of one polypurine DNA strand complexed to a polypyrimidine hairpin peptide nucleic acid (PNA) and was successfully designed to promote Watson-Crick and Hoogsteen base pairing. The P-form helix is underwound, with a base tilt similar to B-form DNA. The bases are displaced from the helix axis even more than in A-form DNA. Hydrogen bonds between the DNA backbone and the Hoogsteen PNA backbone explain the observation that polypyrimidine PNA sequences form highly stable 2:1 PNA-DNA complexes. This structure expands the number of known stable helical forms that nucleic acids can adopt.

Oligonucleotides and modified derivatives, such as phosphorothioates, are being examined as antisense therapeutic agents. An ideal antisense agent would be nuclease-resistant and uncharged to aid cellular penetration. A dramatic deviation from the phosphoribose backbone is PNA, originally developed to be an antigene triplexing agent (*1*). PNA is uncharged and stable toward nucleases, and the achiral PNA backbone (Fig. 1A) can be synthesized by amide-based chemistry.

The first report on PNA demonstrated that a T_{10} PNA polymer bound its complementary A_{10} DNA sequence with a markedly increased T_m (temperature at which 50% of double-stranded DNA is

Glaxo Wellcome, 5 Moore Drive, Research Triangle Park, NC 27709, USA.

*Present address: Amgen Boulder, 3200 Walnut Street, Boulder, CO 80301, USA.

denatured) relative to a $T_{10}{\cdot}A_{10}$ DNA duplex (*1*). The T_{10} PNA displaced the polythymidylate [poly(T)] portion of a DNA duplex target (*1*, *2*) at low ionic strength. Further study showed a tendency for poly(T) PNA to form 2:1 PNA-DNA complexes (*3*). Several groups have designed and synthesized *bis*- or hairpin PNAs to promote triplex formation by tethering two polypyrimidine PNA strands by flexible linkers (*4*, *5*). These PNAs did indeed have increased affinity for single-stranded DNA and a higher rate of strand invasion for double-stranded DNA, relative to single-stranded PNA. To gain insight into the manner in which PNAs complex with DNA to form triplexes, we determined the structure of a nine-base hairpin PNA-DNA complex (Fig. 1B). The structure provides a basis for understanding the high affinity toward nucleic acids exhibited by polypyrimidine PNA and reveals an unusual helix.

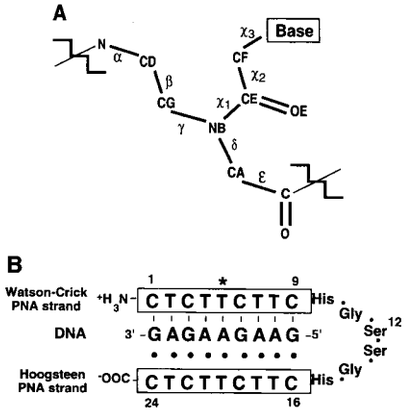

Fig. 1. PNA monomer and PNA_2-DNA_1 complex structures. (**A**) Structure of a PNA monomer. Backbone torsion angles are indicated by Greek letters according to convention (*11*). Carbon positions are designated by A, D, G, E, and F; nitrogen position by B; and oxygen position by E. (**B**) Diagram of the PNA-DNA triplex. DNA was either synthesized by us or purchased from Research Genetics and used without further purification. PNAs were synthesized as described (*4*). The 5-iodo-U base (*T) provided phase information and was a convenient reference point in the electron density. The hexapeptide linker, His-Gly-Ser-Ser-Gly-His, consists of all (L) amino acids.

Table 1. Structure determination. Hairpin PNA-DNA complexes were prepared for crystallization by annealing. Complex at 0.3 mM was mixed with an equal volume of 1.4 M ammonium sulfate and 0.1 M tris-HCl (pH 8.5) and equilibrated at 22°C or 4°C (hanging drop or dialysis buttons) against a reservoir at 1.4 M ammonium sulfate and 0.1 M tris. Crystals were space group $P6_522$, $a = b = 73.38$, $c = 141.28$ Å. Native data were collected at −170°C at the CHESS A-1 beamline to 2.8 Å, with a crystal equilibrated in mother liquor including 25% glycerol. Data were reduced and scaled with DENZO (*16*). 5-Iodo-U derivative crystal data were obtained to a resolution of 2.5 Å at room temperature on a rotating anode with *R*-axis II imaging plates and processed with *R*-axis software. The two iodine atoms in the asymmetric unit were located by difference Patterson maps and confirmed by anomalous difference Pattersons. Initial SIRAS phases to 4.0 Å were calculated and refined with the PHASES program (*17*). Solvent flattening was done to 4.0 Å until convergence. Heavy atom parameters were refined against solvent-flattened phases, iterating the process in increasing shells of resolution to 2.8 Å. A starting model was then built into the electron density with the O graphics program (*18*). The crude model consisting of the bases and backbone provided a mask for noncrystallographic symmetry averaging and phase extension to 2.5 Å. The model was rebuilt into the 2.5 Å map and had a crystallographic *R* factor of 45%. X-PLOR simulated annealing refinement (*19*) with AMBER-based (*20*) parameters with the iodo-U crystal data gave a model with an *R* factor of 22% from 6.0 to 2.5 Å. Thirty-five solvent molecules were identified in $F_o - F_c$ maps by using a 2.8σ cutoff. The final model after individual *B* factor refinement gave an *R* factor of 18.7%. FOM, figure of merit; rms, root mean square.

The structure was solved by using a PNA with an iodinated base to provide initial phase information (Table 1). The SIRAS phases were refined by solvent flattening and noncrystallographic symmetry averaging of the two triplexes in the asymmetric unit. The resulting 2.5 Å electron density map (Fig. 2) clearly shows the positions of

Data collection		
Parameter	Native	5-Iodo-U PNA
Resolution (Å)	2.8	2.5
Total observations	52,364	29,543
Unique reflections	5,723	8,374
Completeness (%)	95	93
R_{sym}* (%)	4.1	4.8
SIRAS statistics		
Statistic	Isomorphous	Anomalous
Phasing power	1.41	3.31
R_{Cullis}†	0.580	
Reflections used (*n*)	5,355	4,149‡
Overall FOM	0.607	
Refinement		
Resolution (Å)	6.0–2.5	
R factor (R_{free})§ (%)	18.7 (23.2)	
Average I/σ to 2.5 Å	6.2	
Reflections with $\|F\| > 2\sigma$	6,857	
Total number of atoms	1,941	
Water molecules (*n*)	35	
rms deviation of bond lengths (Å)	0.014	
rms deviation of bond angles (degrees)	2.43	

*R_{sym} is the agreement between all observations of symmetry-related reflections. †R_{Cullis} (centric) = $\Sigma||F_{PH(obs)}| \pm |F_{P(obs)}|| - |F_{H(calc)}||/\Sigma||F_{PH(obs)}| \pm |F_{P(obs)}||$, where $F_{PH(obs)}$ and $F_{P(obs)}$ are the observed derivative and native structure amplitudes, respectively, and $F_{H(calc)}$ is the calculated heavy atom structure factor. ‡Number of reflections with average anomalous difference >2σ; anomalous difference = $|I^+ - I^-|$, where *I* is intensity. §R_{free} is the cross-validation *R* factor computed for the test set of reflections (8% of the total), which are omitted in the refinement process.

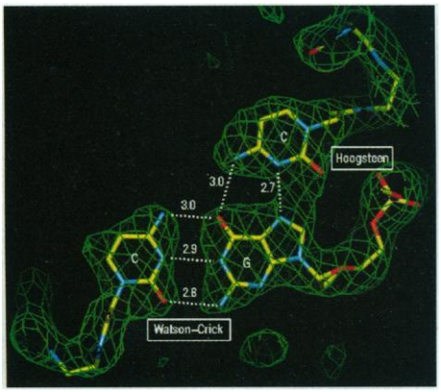

Fig. 2. Representative C·G-C base triplet and its corresponding electron density. The map was calculated with the 2.5 Å symmetry-averaged, solvent-flattened SIRAS phases and is contoured at 1σ.

Table 2. Average torsion angles and helical parameters of PNA-DNA triplex compared with canonical A-DNA and B-DNA. The average angle for each torsion was calculated over both triplexes in the asymmetric unit. Helical parameters for the DNA portion of the triplex were determined with programs described in (*21*).

Molecule	Torsion angles (degrees)									
	α	β	γ	δ	ε	ξ	χ	χ_1	χ_2	χ_3
DNA in triplex	−70	173	61	77	−161	−69	−167			
A-DNA	−50	172	41	79	−146	−78	−154			
B-DNA*	−46	−147	36	157	155	−96	−98			
PNA in WC strand	−103	73	70	93	165			1	−170	89
PNA in H strand	−108	69	69	87	175			1	−175	102

Helical parameters				
	Twist (degrees)	Rise (Å)	Base tilt (Å)	Displacement (Å)	Bases per turn
A-DNA	32.7	2.6	20.0	4.5	11
B-DNA	36.0	3.4	−5.9	−0.1	10
DNA in triplex	22.9	3.4	5.1	6.8	16

*From table 9-3, pp. 230–232, in (*9*).

all the nucleic acid atoms and all of the peptide linker backbone.

The structure revealed a helix (Fig. 3A), which we refer to as P-form for PNA, with helical parameters distinct from either A-form or B-form DNA (Table 2). The P-form helix has a large cavity along the helix axis, reflected by an average base displacement of 6.8 Å (Fig. 3B), compared with 4.5 Å for A-form DNA. The deoxyribose sugars all have a C3′-endo conformation with an average interphosphate distance of 6.0 Å, similar to A-form DNA. This conformation is consistent with the fact that PNAs, including hairpins, bind more tightly to RNA than DNA (5). The tilt of the base triplets, however, is more similar to that of B-form DNA, where the bases are nearly perpendicular to the helix axis. The relative orientation of the Watson-Crick (WC) strands is such that the NH_2-terminus of the PNA is aligned with the 3′ end of the DNA strand. This strand orientation preference is consistent with studies of mixed base sequences and hairpin polypyrimidine PNAs (4–6). The Hoogsteen (H) strand of the PNA is antiparallel to the WC PNA strand, as designed.

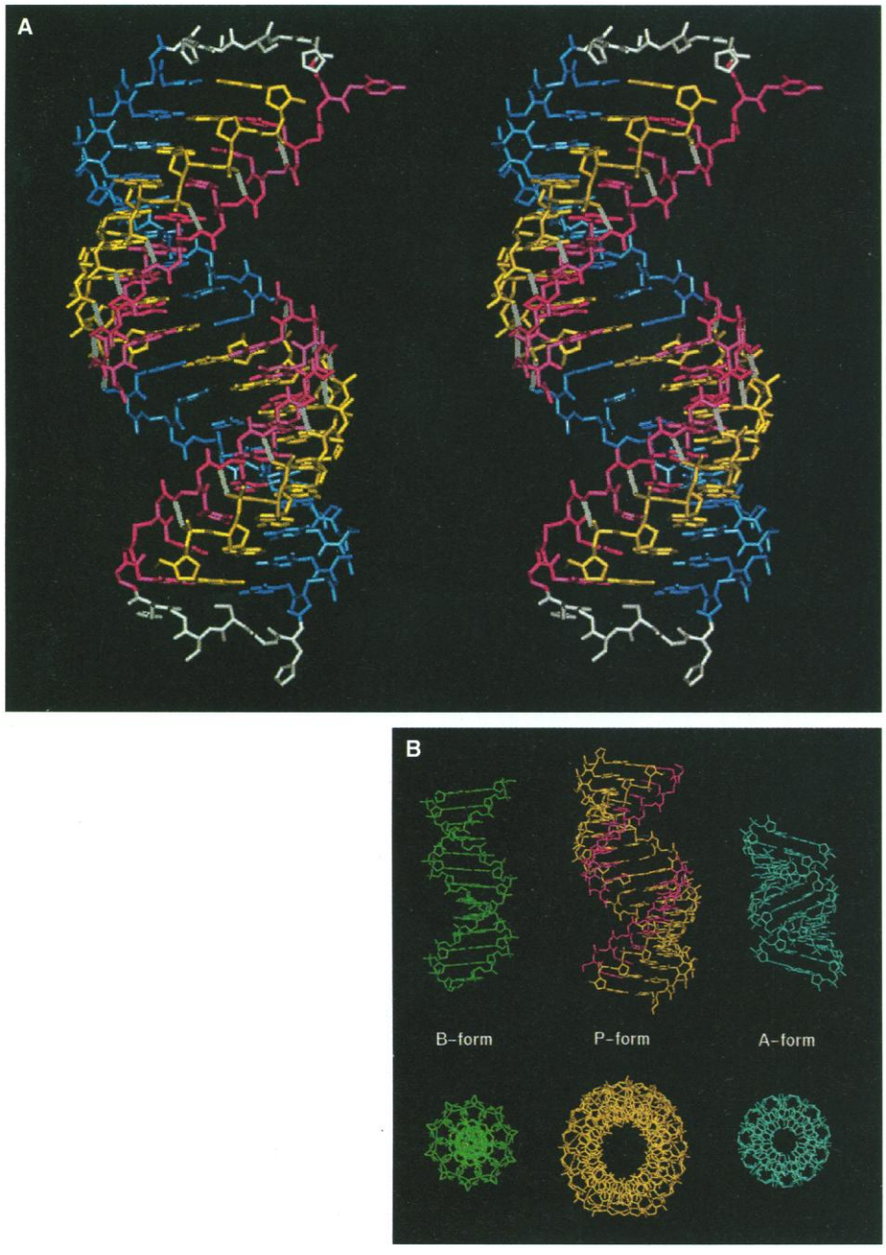

Fig. 3. Structure of the PNA_2-DNA_1 triplex. (**A**) Stereo view of the two triplexes in an asymmetric unit. The DNA in both triplexes is yellow. The magenta strands are the H PNA strands, and the cyan strands are WC PNA strands. Hydrogen bonds between the H PNA and DNA backbone are indicated by white lines. Linker amino acids are drawn in white. (**B**) Comparison of B-, P-, and A-form helices. The H strand of the P-form triplex is magenta. The diameter of the P-form is ~26 Å, whereas that of the A-form is 20 Å. The A- and B-DNA models were built by the program QUANTA (*15*) with the same DNA sequence as the P-form, with each model representing slightly more than one helical turn.

Within the two triplexes in the asymmetric unit all 10 T·A–T triplets and 7 of the 8 C·G-C triplets form with the expected hydrogen-bonding geometry and distances. The purine base of each triplet forms a Watson-Crick base pair with the pyrimidine base on one PNA strand and a Hoogsteen base pair with the pyrimidine on the other strand. This type of (Y·R-Y) interaction has been seen in nuclear magnetic resonance (NMR) studies of oligonucleotide triplexes (7) and predicted for PNA_2-DNA_1 complexes (3–6). The average distance between the N3 atoms of the Hoogsteen cytosines and N7 atoms of the guanines is 2.8 Å, indicating that those atoms must be hydrogen bonded (Fig. 2). The N3 of the Hoogsteen cytosines must be significantly protonated even though the pK_a (where K_a is the acidity constant) of a free cytosine is 4.2 and this triplex was crystallized at pH 8.5. The one cytosine that does not make the intended Hoogsteen interaction, cytosine^{16}, swings out to form an edge to face interaction with cytosine^{6} of a crystallographically related complex.

The pattern of base stacking along the Watson-Crick portion of the P-form triplex resembles that found in an A-form DNA duplex (8), despite the much larger displacement of the bases from the P-form helix axis. The 2-keto groups of the Hoogsteen pyrimidines stack over the imidazole ring of the preceding DNA purine. These interactions are consistent with those in

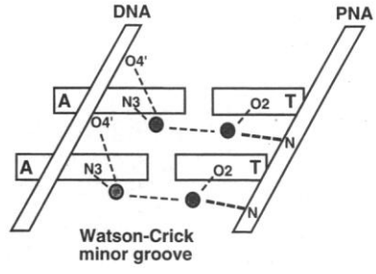

Fig. 4. Minor groove interactions in an A-T region. Solvent molecules are black spheres. Hydrogen bonds are drawn as dashed lines. The DNA backbone is filled in gray, and the PNA is white. A water molecule links each WC PNA backbone amide proton to the O2 keto oxygen of the preceding pyrimidine residue on that strand. A second row of waters bridges the first row with the ribose O4′ atom and adenine N3 atoms. As a consequence of this hydration network, the WC PNA and DNA backbones are linked together.

which polar atoms are stacked over the aromatic rings of adjacent bases (9).

The triplex structure revealed a strong interaction between the DNA backbone and the PNA backbone of the Hoogsteen strand. The O1P oxygen from each phosphate group of the DNA backbone hydrogen bonds to the amide proton of each residue of the PNA backbone of the H strand with an average distance of 2.85 Å. There are extensive van der Waals interactions between the two strands. A total of 180 $Å^2$ out of 260 $Å^2$ of surface area per H PNA residue is buried on complex formation with a DNA residue. In contrast, the WC PNA backbone makes no direct interactions with the DNA.

There are two triplexes stacked in the asymmetric unit, related by approximate twofold symmetry perpendicular to the helical axis (Fig. 3A). As a result, the two PNA backbones form a nearly continuous helix with the carboxylate of the COOH-terminus of each of the H PNA chains forming a salt bridge with the NH_2-terminus of each WC PNA chain. The amino acid linkers sterically block any potential stacking between the top of each triplex and any other triplex, preventing formation of an infinite helix.

The linker peptide was chosen to be both flexible and to impart solubility. Each linker in the asymmetric unit adopts a different conformation although all phi-psi angles are within sterically allowed regions. The average main-chain temperature factor for the amino acid linker region is higher than that of the PNA backbone, further indicating that the linker is relatively flexible and does not impose a particular conformation on the triple helix.

There are 35 clearly defined water molecules. One class of water molecules binds in the minor groove to both the amide hydrogen of the WC PNA backbone, with an average distance of 2.9 Å, and to the O2 oxygen of the preceding pyrimidine base, with an average distance of 3.0 Å (Fig. 4). These water molecules stabilize the residues in the WC PNA strand in a conformation that is nearly identical to the H PNA strand. They were the strongest peaks in the $F_o - F_c$ difference maps (where F_o and F_c are the observed and calculated structure factors, respectively) and were present in the original electron density. Another set of water molecules bridges the first set to the N3 atoms of the adenine bases in the minor groove (Fig. 4). In the case of C·G-C triplets, there is no corresponding water, presumably because of steric interference by the exocyclic amino group of the guanine. These waters all interact to stabilize the P-form helix. Minor groove solvent networks have been observed to stabilize B-form DNA in A-T rich regions by the so-called spine of hydration (*10*). In the P-form major groove, exocyclic heteroatoms of the pyrimidines are generally solvated with either one or two water molecules.

The structure of the complex explains a number of biochemical and biophysical properties of PNAs. The structure provides direct confirmation that PNAs can recognize nucleic acids by both Watson-Crick and Hoogsteen hydrogen bonding. The conformation of the PNA and DNA backbones that accomodates both duplex and triplex interactions is elucidated by the structure (Table 2). The tight association between the DNA strand and the H PNA strand is stabilized both by hydrogen bonds between the DNA phosphate oxygens and the PNA amides and by extensive van der Waals interactions that lock the structure in the P-form helical conformation. Hydrogen bonds to solvent molecules in the minor groove strengthen the P-form Watson-Crick PNA-DNA interactions. This stable triplex accounts for the strong tendency of polypyrimidine PNA sequences to associate with polypurine DNA in a 2:1 ratio and also accounts for the increased T_m of these complexes compared with DNA duplex and triplex sequences.

The NMR structure of a mixed sequence PNA-RNA duplex has been recently reported (*11*) and was described to be most consistent with an A-form helix. The PNA χ_1 torsion angle is very similar in both the NMR duplex and x-ray triplex structures, so that the carbonyl of the tertiary amide points toward the COOH-terminus of the PNA strand. The duplex and triplex structures differ at the α and ε torsion angles, which specify the orientation of the interresidue amide carbonyl. In the refined NMR duplex structures, the predominant orientation of the backbone carbonyl oxygen is more toward the PNA NH_2-terminus, whereas in the P-form triplex the carbonyl oxygen points toward the PNA COOH-terminus. In the triplex crystal structure, the conformation of the PNA residues is nearly identical in the WC strand and the H strand, suggesting that it is a stable conformation consistent with forming either a WC duplex or a triplex. The observed differences in backbone conformation between the NMR duplex and the x-ray triplex could arise from factors such as differences in sequence length and composition, solution compared with crystal, and an RNA compared with a DNA target.

DNA triplex structures have been studied predominantly by NMR. In some studies the triplex is described as being more similar to B-form (*7*), whereas other studies indicate it is more similar to A-form (*12*), as reported for the original fiber diffraction studies of poly(dT) · poly(dA) · poly(dT) (*13*). Base triplets have been observed in a number of crystal structures, but the extent of the "helix" is limited to one or two base triplets, usually resulting from an interaction between an overhanging base with a duplex strand (*14*). Clearly, triplex formation may require features that are not easily accommodated by either classical A- or B-form helices. The PNA_2-DNA_1 triplex forms a previously unknown helix that expands the library of known nucleotide helical structures. This study suggests that there may be additional classes of stable DNA triplexes yet to be discovered.

REFERENCES AND NOTES

1. P. E. Nielsen, M. Egholm, R. H. Berg, O. Buchardt, *Science* **254**, 1497 (1991).
2. D. Y. Cherny *et al.*, *Proc. Natl. Acad. Sci. U.S.A.* **90**, 1667 (1993); N. J. Peffer *et al.*, *ibid.*, p. 10648.
3. M. Egholm, O. Buchardt, P. E. Nielsen, R. Berg, *J. Am. Chem. Soc.* **114**, 1895 (1992); M. Egholm, P. E. Nielsen, O. Buchardt, R. H. Berg, *ibid.*, p. 9677; S. K. Kim *et al.*, *ibid.* **115**, 6477 (1992).
4. J. A. Josey *et al.*, in preparation.
5. M. Egholm *et al.*, *Nature* **365**, 566 (1993); M. C. Griffith *et al.*, *J. Am. Chem. Soc.* **117**, 831 (1995); M. Egholm *et al.*, *Nucleic Acids Res.* **23**, 217 (1995).
6. P. E. Nielsen, M. Egholm, O. Buchardt, *J. Mol. Recognit.* **7**, 165 (1995).
7. R. Macaya, E. Wang, P. Schultze, V. Sklenar, J. Feigon, *J. Mol. Biol.* **225**, 755 (1992); I. Radhakrishnan and D. J. Patel, *Structure* **2**, 17 (1994).
8. W. N. Hunter, B. Langlois-D'Estaintot, O. Kennard, *Biochemistry* **28**, 2444 (1989).
9. W. Saenger, *Principles of Nucleic Acid Structure* (Springer-Verlag, New York, 1984), pp. 132–133.
10. H. R. Drew and R. E. Dickerson, *J. Mol. Biol.* **151**, 535 (1981).
11. S. C. Brown, S. A. Thomson, J. M. Veal, D. G. Davis, *Science* **265**, 777 (1994).
12. C. M. de los Santos, D. Rosen, D. J. Patel, *Biochemistry* **28**, 7282 (1989); K. Umemoto, M. H. Sarma, G. Gupta, J. Luo, R. H. Sarma, *J. Am. Chem. Soc.* **112**, 4539 (1990).
13. S. Arnott and E. Selsing, *J. Mol. Biol.* **88**, 509 (1974).
14. L. Van Meervelt *et al.*, *Nature* **374**, 742 (1995).
15. QUANTA, 4.0; developed by Molecular Simulations, Burlington, MA (1994).
16. Z. Otwinowski, in *Proceedings of the CCP4 Study Weekend: Data Collection and Processing*, Daresbury, England, 29 and 30 January 1993; L. Sawyer, N. Isaacs, S. Bailey, Eds. (Science and Engineering Research Council Daresbury Laboratory, England, 1993), pp. 56–62.
17. W. Furey and S. Swaminathan, *Am. Crystallogr. Assoc. Program Abstr.* **18**, 73 (1990).
18. A. T. Jones and M. Kjeldgaard, O manual, version 5.9.1 (University of Uppsala, Uppsala, Sweden, 1994).
19. A. T. Brunger, X-PLOR manual, version 3.1 (Yale Univ. Press, New Haven, 1987).
20. S. J. Weiner, P. A. Kollman, D. T. Nguyen, D. A. Case, *J. Comput. Chem.* **7**, 230 (1986).
21. M. S. Babcock, E. P. D. Pednault, W. K. Olson, *J. Biomol. Struct. Dyn.* **11**, 597 (1993).

22. We thank S. C. Brown for discussions, F. Hassman for synthesis of DNA, J-M. Ding and D. Rose for analysis of dissolved crystals, and S. Ginell and L. Keefe (Brookhaven National Laboratory) for help in data collection on a brominated crystal. The Brookhaven Protein Data Bank accession code for the PNA-DNA triplex is 1PNN.

7 June 1995; accepted 18 October 1995